


# A biophysical model of striatal microcircuits suggests $\theta$ -rhythmically interleaved $\gamma$ and $\beta$ oscillations mediate periodicity in motor control

Julia A. K. Chartove<sup>1\*</sup>, Michelle M. McCarthy<sup>1</sup>, Benjamin R. Pittman-Polletta<sup>1</sup>,  
Nancy J. Kopell<sup>1</sup>

<sup>1</sup> Department of Mathematics & Statistics, Boston University, Boston, MA

 These authors co-mentored this work

\* [jchartove@bu.edu](mailto:jchartove@bu.edu)

## Abstract

Striatal oscillatory activity is associated with movement, reward, and decision-making, and observed in several interacting frequency bands. Local field potential (LFP) recordings in rodent striatum show dopamine- (DA-) and reward-dependent transitions between two states: a “spontaneous” state involving  $\beta$  ( $\sim 15\text{-}30$  Hz) and low  $\gamma$  ( $\sim 40\text{-}60$  Hz), and a state involving  $\theta$  ( $\sim 4\text{-}8$  Hz) and high  $\gamma$  ( $\sim 60\text{-}100$  Hz) in response to DAergic agonism and reward. The mechanisms underlying these rhythmic dynamics, their interactions, and their functional consequences are not well understood. In this paper, we propose a biophysical model of striatal microcircuits that comprehensively describes the generation and interaction of these rhythms, as well as their modulation by DA. Building on previous modeling and experimental work suggesting that striatal projection neurons (SPNs) are capable of generating  $\beta$  oscillations, we show that networks of striatal fast-spiking interneurons (FSIs) are capable of generating  $\theta$  and  $\gamma$  rhythms. Our model consists of three interconnected populations of single or double compartment Hodgkin-Huxley neurons: a feedforward network of FSIs exhibits a D-type potassium current as well as DA-modulated gap junctional and inhibitory connectivity, and two networks of SPNs exhibit an M-type potassium current and express either

excitatory D1 or inhibitory D2 DA receptors. Under simulated low DAergic tone the FSI network produces low  $\gamma$  band oscillations, while under high DAergic tone the FSI network produces high  $\gamma$  band activity nested within a  $\theta$  oscillation. SPN networks produce  $\beta$  rhythms in both conditions, but under high DAergic tone, this  $\beta$  oscillation is interrupted by  $\theta$ -periodic bursts of  $\gamma$ -frequency FSI inhibition. Thus, in the high DA state, packets of FSI  $\gamma$  and SPN  $\beta$  alternate at a  $\theta$  timescale. In addition to a mechanistic explanation for previously observed rhythmic interactions and transitions, our model suggests a hypothesis as to how the relationship between DA and rhythmicity impacts motor function. We hypothesize that high DA-induced periodic FSI  $\gamma$ -rhythmic inhibition enables switching between  $\beta$ -rhythmic SPN cell assemblies representing the currently active motor program, and thus that DA facilitates movement by allowing for rapid, periodic shifts in motor program execution.

## Author summary

Striatal oscillatory activity is associated with movement, reward, and decision-making, and observed in several interacting frequency bands. The mechanisms underlying these rhythmic dynamics, their interactions, and their functional consequences are not well understood. In this paper, we propose a biophysical model of striatal microcircuits that comprehensively describes the generation and interaction of striatal rhythms, as well as their modulation by DA. Our model suggests a hypothesis as to how the relationship between DA and rhythmicity impacts the function of the motor system, enabling rapid, periodic shifts in motor program execution.

## Introduction

As the largest structure of the basal ganglia network, the striatum is essential to motor function and decision making. It is the primary target of dopaminergic (DAergic) neurons in the brain, and its activity is strongly modulated by DAergic tone. Disorders of the DA and motor systems, such as Parkinson's, Huntington's, Tourette's, and many others, result in abnormal network activity within striatum [1]. Rhythmic activity is observed in both striatal spiking and local field potential, and oscillations in the

striatum are correlated with voluntary movement, reward, and decision-making in healthy individuals [2–4], while disruptions of these rhythms are biomarkers of mental and neurological disorders [1, 5, 6]. However, the mechanisms of these oscillations, and their role in motor behavior and its dysfunctions, remain poorly understood.

Four oscillatory bands in particular are frequently observed in striatal local field potential:  $\theta$  (4-7 Hz),  $\beta$  (8-30 Hz), low  $\gamma$  (50-60 Hz), and high  $\gamma$  (70-80 Hz) [2, 7, 8]. Power in these bands consistently correlates with responses to task parameters such as motor initiation, decision making, and reward [2–4, 6]. Power in the  $\beta$  band is elevated in Parkinson’s disease and correlates with the severity of bradykinesia [1]. In the healthy basal ganglia,  $\beta$  and  $\gamma$  activity are inversely correlated and differentially modulated by slower basal ganglia rhythmic activity, suggesting that the balance of these distinct oscillatory dynamics is important to healthy motor function [8]. In rat striatum *in vivo*, spontaneous  $\beta$  and low  $\gamma$  oscillations transition to  $\theta$  and high  $\gamma$  dynamics upon reward receipt and with administration of DA agonist drugs [2]; similarly, in rat caudate and putamen, DAergic agonists produce robust low-frequency modulation of high  $\gamma$  amplitude [7].

In this paper, we propose a biophysical model of striatal microcircuits that comprehensively describes the generation and interaction of these rhythms, as well as their modulation by DA. Our simulations capture the dynamics of networks of striatal fast-spiking interneurons (FSIs) and striatal projection neurons (SPNs), using biophysical Hodgkin-Huxley type models. SPNs, responsible for the output of the striatum, make up 95% of striatal neurons in rodents [9]. SPN firing is regulated by relatively small populations of striatal interneurons, including fast spiking interneurons (FSIs), which strongly inhibit SPNs. Our model FSIs exhibit a D-type potassium current [10], and our model SPNs exhibit an M-type potassium current [11]. Both cell types are modulated by DAergic tone: FSIs express the excitatory D1 DA receptor [12], while two distinct subpopulations of SPNs express exclusively the D1 or the inhibitory D2 receptor subtype. We modeled both SPN subpopulations, with high simulated DAergic tone increasing and decreasing D1 and D2 SPN excitability, respectively. To model DA effects on the FSI network, we simulated three salient experimentally observed effects: increased excitability [12] and gap junction conductance [13], and decreased inhibitory conductance [12]. Both gap junctions and inhibition are known to

play a role in the generation of rhythmic activity [14].

Our previous experimental and modeling work suggests that striatal SPN networks can produce a  $\beta$  (15-25 Hz) oscillation locally [15]. Our current model demonstrates that FSI networks can produce  $\theta$ , low  $\gamma$ , and high  $\gamma$  oscillations. A fast-activating, slow-inactivating potassium current (the D-type current) allows FSIs to produce  $\gamma$  and  $\theta$  rhythms in isolation, and network interactions make these rhythms, otherwise highly susceptible to noise, robust. In our simulations, DA induces a switch between two FSI network states: a low DA state exhibiting persistent low  $\gamma$  rhythmicity, and a high DA state in which a  $\theta$  oscillation modulates high  $\gamma$  activity. As a result of FSI inhibition of SPNs, DA induces a switch in striatal dynamics, between a low DA state in which low  $\gamma$  and  $\beta$  rhythms coexist, and a high DA state in which bursts of FSI high  $\gamma$  and SPN  $\beta$  rhythms alternate, nested within (and appearing at opposite phases of) an FSI  $\theta$  rhythm.

Thus, our model generates a hypothesis as to how observed relationships between DA and rhythmicity impact the function of the motor system. Namely, DA appears to encourage or permit periodic motor program switching, by allowing the emergence of an FSI-mediated  $\theta$ -modulated  $\gamma$  rhythm that breaks up the “stay” signal mediated by SPN  $\beta$  rhythms [16].

## Results

### Single model FSIs produce $\theta$ -nested $\gamma$ rhythms whose power and frequency is modulated by excitation

We modified a previous single-compartment striatal FSI model [17] by adding a dendritic compartment (shown to be an important determinant of gap-junction mediated synchrony [18]) and increasing the conductance of the D-type K current to 6  $mS$ . Previous work showed that two characteristic attributes of FSI activity *in vitro* – stuttering and  $\gamma$  resonance (defined as a minimal tonic firing rate in the  $\gamma$  frequency range) – are dependent on the D-current. Our modified FSI model successfully reproduced these dynamics as well as revealing other dynamical behaviors (Fig. 1).

With increasing levels of tonic applied current ( $I_{app}$ ), our model FSI transitions from

**Fig 1.** Behavior of single model FSI over a range of inputs and D-current conductances. (A) i. A single model FSI with low tonic excitation ( $8\mu A/cm^2$ ) spikes at a low  $\gamma$  frequency nested in slow bursting, while a single model FSI with high tonic excitation ( $20\mu A/cm^2$ ) spikes at a high  $\gamma$  nested in slow bursting. ii. Power spectral density of voltage traces in (A)i, comparing low and high levels of tonic excitation. (B) i. Single model FSI with tonic excitation ( $10\mu A/cm^2$ ) and weak Poisson noise ( $\lambda = 500$ ) spikes at  $\gamma$  nested in  $\theta$ , while a single model FSI with tonic excitation ( $10\mu A/cm^2$ ) and strong Poisson noise ( $\lambda = 5500$ ) has limited low-frequency content. ii. Power spectral density of voltage traces in (B)i, comparing low and high levels of noise. (C) Three-dimensional false-color plot demonstrating the dependence of the bursting regime on  $g_d$  and  $I_{app}$ . (D) Three-dimensional false-color plot demonstrating the dependence of firing rate on  $g_d$  and  $I_{app}$ .

quiescence to (periodic) bursting to periodic spiking. The bursting regime, of particular interest in this work, is dependent on the level of tonic excitation (Fig. 1A,C,D), the level of noise in excitatory drive (Fig. 1B & 2C), and, centrally, the D-current conductance (Fig. 1C,D). With lower levels of D-current (as used in previous FSI models [10,17,19]), bursting is aperiodic. For sufficiently large D-current conductance, FSI bursting occurs for a broad range of applied currents ( $I_{app}$  over  $8\text{ uA/cm}^2$ , Fig. 1C,D).

**Fig 2.**  $I_D$ , applied current, and applied noise determine interburst and intraburst frequency of FSI spiking. (A) Plot of the minimal firing rate within a burst of a single model FSI with and without  $I_D$ . (B) Plot of the maximal inter-burst ( $\delta$ ) frequency and intraburst ( $\gamma$ ) firing rate of a single model FSI as the time constant of inactivation of  $I_D$  is increased. (C) Plot of the inter-burst frequency and power of a single model FSI as noise is applied. For B and C  $I_{app} = 10\mu A/cm^2$ .

The frequency of bursting depends on the decay time constant of the D-type potassium current ( $\tau_D$ ); in the absence of noise, it is in the  $\delta$  frequency range for physiologically relevant  $\tau_D$  ( $< \sim 200$  ms, Figure 1A,C, 2B). Note that  $\tau_D$  changes the inter-burst interval without changing the timing of spikes within a burst (Fig. 2B). Burst frequency also increases with increasing tonic excitation (Fig. 1,A,C), and increases to  $\theta$  frequencies with small amounts of noise (Fig. 1B, 2C), which decrease the interburst interval. However, large amounts of noise abolish rhythmic bursting altogether (at least in single cells, Fig. 1B).

As shown previously [17], the FSI model's  $\gamma$  rhythmic intraburst spiking arises from its minimum firing rate, which is also set by the D-current conductance (Fig. 2A); when this conductance is zero, the model has no minimum firing rate (Fig. 2A). As this

conductance is increased, the minimum firing rate also increases. Thus, our choice of 87  
D-current reflects not only our interest in the bursting regime, but also our desire to 88  
match experimental observations of striatal  $\gamma$  frequency [2, 17]. FSI spiking frequency 89  
also increases with tonic drive (Figure 1A,D). Since simulated DA acts on our FSI 90  
model by increasing tonic excitation, DA causes a switch in model FSI spiking from low 91  
 $\gamma$  rhythmicity to  $\delta$ -modulated high  $\gamma$  rhythmicity. Below, we demonstrate that the FSI 92  
 $\gamma$  is determined by this single-cell rhythmicity and is mostly independent of the 93  
timescale of inhibitory synapses. 94

In summary, a single model FSI displays low-frequency-nested  $\gamma$  oscillations, 95  
dependent on the D-type current, under a wide range of tonic excitation levels. Both low 96  
frequency power and  $\gamma$  frequency increase with tonic excitation. While noise increases 97  
the frequency of the slower rhythm from  $\delta$  to  $\theta$ , it also diminishes the power of this 98  
rhythm in the single cell. Below we demonstrate that all of these effects are also present 99  
in a network of FSIs, with the key difference that the  $\theta$  rhythm becomes robust to noise. 100

## FSI networks produce DA-dependent $\theta$ and $\gamma$ rhythms 101

To determine if  $\theta$  and  $\gamma$  oscillations persist in networks of connected FSIs, and how DA 102  
could modulate network dynamics, we simulated a network of 100 model FSIs connected 103  
randomly (with an independent connection probability of 0.3 for each type of 104  
connection) by both inhibitory synapses and gap junctions. We also implemented three 105  
salient and experimentally observed effects of DA on FSI networks: increased tonic 106  
excitation of individual FSIs [12], increased gap junction conductance between FSIs [13], 107  
and decreased inhibitory conductance between FSIs [12] (see Methods). 108

Unlike in single cells, FSI network  $\theta$  rhythmicity is dependent on sufficient levels of 109  
tonic excitation: at low levels of tonic input ( $I_{app} < \approx 1 \mu A/cm^2$ ), the FSIs do not attain 110  
enough synchrony for a strong network  $\theta$  (Fig. 3Aii). As in single cells, FSI network  $\theta$  111  
power increases with tonic input strength (Fig. 3Aii). Sufficiently strong gap junction 112  
coupling is also a requirement for the FSI network to attain sufficient synchrony to 113  
produce  $\theta$  rhythmicity (Fig. 3Cii), protecting the FSI network  $\theta$  rhythm from the effects 114  
of noise (as in [14]). Finally, inhibitory synaptic interactions between FSIs have a 115  
desynchronizing effect that interferes with network  $\theta$ , and increasing inhibitory 116

conductance within the FSI network decreases power in the  $\theta$  band (Fig. 3Bii). 117

**Fig 3.** FSI network rhythms change with background excitation and synaptic strength. Power and frequency of  $\theta$  and  $\gamma$  rhythms in FSI network mean voltage as a function of (A) tonic input current, (B) GABA<sub>A</sub> conductance, and (C) gap junction conductance.. The parameters not being varied in plots A-C are held at the high DA values ( $g_{\text{gap}} = 0.2\text{mS}$ ,  $g_{\text{syn}} = 0.005\text{mS}$ ,  $I_{\text{app}} = 16\mu\text{A}/\text{cm}^2$ ,  $\tau_{\text{gaba}} = 13\text{ms}$ ). (D) Gamma frequency as a function of GABA<sub>A</sub> synaptic time constant and level of dopamine. 118

FSI network  $\gamma$  power and frequency both increase with tonic input strength (Fig. 3Ai), and, like the network  $\theta$ , the network  $\gamma$  rhythm is dependent on sufficient gap junction conductance and is disrupted by inhibition (Fig. 3B & C, i). 119 120

To explore FSI network dynamics that might be observed during normal fluctuations in DA during goal-directed tasks [20], we simulated FSI network activity under two conditions, simulated low (or baseline) and high DAergic tone. During simulated low DAergic tone, characterized by low levels of FSI tonic excitation and gap junction conductance, and high levels of inhibitory conductance, the network produces a persistent low frequency  $\gamma$  oscillation ( $\sim 55$  Hz) in the model LFP (the mean voltage of the FSI network, Fig. 4Bi-Di). The raster plot of FSI spike times (Fig. 4Eii) shows that individual FSIs exhibit sparse spiking in the low DA state. Although individual FSIs exhibit periodic spike doublets or bursts ( $\gamma$ -paced and entrained to the network  $\gamma$ ) that recur at  $\theta$  frequency, the timing of these bursts is independent (Fig. 4Ei). Therefore, while  $\theta$  power is present at the level of individual FSIs, there is not sufficient synchrony for it to appear in the network (Fig. 4Di). 121 122 123 124 125 126 127 128 129 130 131 132

During simulated high DAergic tone, characterized by high levels of tonic excitation and gap junction conductance and low levels of inhibitory conductance, network activity is much more structured: a strong 70 Hz  $\gamma$  rhythm, phase-modulated by a 5 Hz  $\theta$  rhythm, are evident in both the simulated LFP and network raster plots (Fig. 4Bii-Eii, right). In this state, active FSIs spike at the same phase of both  $\theta$  and  $\gamma$ , producing dual (and nested) network rhythms (Fig. 4iii). 133 134 135 136 137 138

To explore whether the  $\gamma$  rhythms observed in the FSI network are generated by inhibitory interactions, we examined the dependence of  $\gamma$  frequency on the time constant of GABA<sub>A</sub> inhibition, as the characteristic frequency of canonical interneuron network  $\gamma$  (ING) has been shown to depend on this time constant [21]. The frequency 139 140 141 142

**Fig 4.** FSI network activity and rhythms are altered by DA.

(A) Schematics showing the major alterations to the FSI network during the baseline (i) and high (ii) DAergic tone conditions. (B) Mean voltage for the FSI network in the two conditions. (C) Spectrograms of (B). (D) Solid line: Average power spectral density of FSI population activity. Dashed line: Average power spectral density of all individual FSI voltage traces in the network. (E) Raster plots of FSI network activity at second and subsecond timescales.

of the  $\gamma$  rhythm produced under low DA conditions decreased with increases in the 143  
GABA<sub>A</sub> time constant (Fig. 3D), suggesting this rhythm is ING-like. However, the  $\gamma$  144  
produced under high DA conditions had a frequency that was not highly dependent on 145  
the inhibitory time constant, suggesting that this  $\gamma$  rhythm is mechanistically different 146  
from previous ING models, being generated by synchronous  $\gamma$  frequency bursts in 147  
individual cells, as opposed to inhibitory interactions. 148

### SPN networks generate DA-dependent $\beta$ oscillations 149

Previous work by our group found that robust  $\beta$  oscillations can emerge from inhibitory 150  
interactions in networks of model striatal SPNs [15]. The interaction of synaptic 151  
GABA<sub>A</sub> currents and intrinsic M-currents promotes population oscillations in the  $\beta$  152  
frequency range; their  $\beta$  timescale is promoted by the M-current, which allows rebound 153  
excitation at  $\sim 50$  ms in response to synaptic inhibition. Excitation of these neurons 154  
increases  $\beta$  power (see Methods). This previous work explored the transition from a 155  
healthy to a parkinsonian state with pathologically low levels of striatal DA. To explore 156  
the generation of  $\beta$  rhythmicity during normal fluctuations in DAergic tone, we 157  
simulated two independent networks of 100 D1 receptor expressing (“direct pathway”) 158  
SPNs and 100 D2 receptor expressing (“indirect pathway”) SPNs. Model SPNs are 159  
single compartment cells expressing the Hodgkin-Huxley spiking currents and the 160  
M-type potassium current, interconnected all to all by inhibitory GABA<sub>A</sub> synapses 161  
(connection probability 1). We simulated the effects of DA on model D1 and D2 SPNs 162  
by increasing and decreasing their levels of tonic excitation, respectively (whether DA 163  
generates a positive or negative applied current was the only difference between D1 and 164  
D2 expressing SPNs in our model; Fig. 5i and ii; see Methods). Paradoxically, in the 165  
absence of FSI input, neither population was sufficiently excited to exhibit spontaneous 166  
spiking under low DA conditions (Fig. 5i); under high DA conditions, D1 SPNs 167



exhibited persistent  $\beta$  rhythmicity at  $\sim 15$  Hz (Fig. 5ii). 168

**Fig 5.** FSIs paradoxically excite and pattern SPN network activity.

(A) Schematics showing the major alterations during the baseline (i, iii) and high (ii, iv) DAergic tone conditions, in an isolated SPN network (i, ii) and a combined FSI-SPN network (iii,iv). (B) Mean voltages for the D1 and D2 SPN populations in the two conditions. (C) Spectrograms of mean voltage for the D1 population (upper) and D2 population (lower). (D) Average power spectral density of D1 and D2 population activity. (E) Raster plots of SPN population activity.

## FSI network $\gamma$ and $\theta$ oscillations rhythmically modulate SPN 169

### network $\beta$ oscillations only in high DA state 170

To understand the interactions between FSI and SPN networks, and between  $\beta$ ,  $\gamma$ , and  $\theta$  rhythms, we simulated a combined FSI-SPN striatal microcircuit, in which 100 model 171  
FSIs randomly inhibited independent networks of 100 D1 and 100 D2 SPNs (connection 172  
probability from FSIs to D1 or D2 SPNs of 0.1). FSIs were interconnected by gap 173  
junctions and inhibitory synapses (connection probability 0.3 for each). D1 and D2 174  
SPNs were connected by all to all inhibitory synapses within (connection probability 1) 175  
but not across populations. There were no connections from SPNs back to FSIs [22]. 176  
177

During simulated baseline DAergic tone, we modeled D1 and D2 SPNs as being 178  
equally excitable, with equal firing rates matching *in vivo* observations [23] while under 179  
the influence of FSI inhibition. The presence of FSIs is necessary for the SPNs to fire in 180  
the low dopamine state (Fig. 5iii); this paradoxical excitatory effect of GABAergic 181  
input arises because SPNs can be excited via post-inhibitory rebound, as demonstrated 182  
in previous work. [15]. Both SPN networks produce a  $\beta$  rhythm (15 Hz), while the FSI 183  
network produces a low (50 Hz)  $\gamma$  (Fig. 5iii & 6i). The generation of low  $\gamma$  rhythms by 184  
the FSIs and  $\beta$  by the SPNs matches observations of striatal rhythmicity in resting 185  
healthy animals *in vivo* [2]. Our model suggests that these  $\gamma$  and  $\beta$  rhythms are 186  
independently generated by FSI and SPN networks, respectively. 187

**Fig 6.** In the high DA state, packets of FSI  $\gamma$  and SPN  $\beta$  alternate at a  $\theta$  timescale.

(A) Schematics showing the major alterations to the striatal network during the baseline (i) and high (ii) DAergic tone conditions. (B) LFP surrogates for low and high DAergic tone conditions. (C) Spectrograms of LFP surrogates. (D) Wavelet-filtered  $\beta$  and  $\gamma$  oscillations from the population activity in (B). (E) Schematic of oscillatory activity during low and high DAergic tone conditions, with proposed functional impact on ensemble activity.

During simulated high DAergic tone, an FSI-mediated high ( $\sim 70$  Hz)  $\gamma$  and an SPN-mediated  $\beta$  are observed during opposite phases of an ongoing FSI network  $\theta$  rhythm (Fig. 5iv & 6ii). During the peak of the  $\theta$ , the incoming  $\gamma$  frequency input from the FSIs silences the SPNs. When the FSIs are silent during the  $\theta$  trough, both D1 and D2 SPN populations are sufficiently excited to produce a  $\beta$  rhythm. Thus, while the SPNs cannot entrain to the  $\gamma$  frequency of FSI inhibition, they are modulated by the FSI-generated  $\theta$  rhythm.

## Discussion

Our model suggests that DAergic tone can produce a transition between two dynamical states in striatal GABAergic networks. In the baseline DAergic tone state, ongoing low  $\gamma$  (50-55 Hz) and  $\beta$  (15 Hz) oscillations are generated by striatal FSI network and SPN networks, respectively (Fig. 6i). In the high DAergic tone state, packets of FSI-mediated high  $\gamma$  (65-70 Hz) and SPN-mediated  $\beta$  (10-20 Hz) rhythms alternate at  $\theta$  ( $\sim 5$  Hz) frequency (Fig. 6ii). Our results make predictions about the generation of striatal rhythms, have implications for the role of FSIs in regulating the activity of SPNs and suggest an underlying mechanism for the temporal dynamics of motor program selection and maintenance (Fig. 6E).

### Mechanisms of $\gamma$ and $\delta/\theta$ oscillations in single FSIs

Prior work has shown  $\gamma$  oscillations in striatal FSIs arising from an interaction between the spiking currents and the spike frequency adaptation caused by the potassium D-current, which produces a minimum FSI firing rate in the  $\gamma$  range [17,24]. The frequency of the FSI  $\gamma$  depends on excitatory drive to the FSIs, which in our model leads to the modulation of  $\gamma$  frequency by DA, a phenomenon also observed in striatal  $\gamma$  oscillations *in vivo* [25–28].

Prior work has also suggested that the D-current is responsible for the bursting or stuttering behavior of FSIs, in which brief periods of high frequency activity are interspersed with periods of quiescence [10]. However, regularities in these periods of quiescence have not been previously observed. Thus, the present study is novel in its description of the generation of low-frequency rhythms by FSIs with high levels of

D-current conductance; FSIs have previously been characterized solely as generators of  $\gamma$  oscillations. Our model predicts that FSI-mediated slow rhythms depend on a high level of D-current conductance. In our model, the D-current is activated by burst spiking, e.g., at  $\gamma$  frequency, and hyperpolarizes the cell for roughly a  $\theta$  period due to its long time constant of inactivation. Though individual cells produce a  $\delta$  rhythm, the frequency of the resulting  $\theta$  oscillation in the network is robust to changes in excitatory drive. This transition to a higher rhythm in the network is likely a result of gap-junction induced synchrony driving burst frequency higher while maintaining robustness to noise. Notably, this study is also a novel demonstration of the generation of both  $\theta$  and  $\gamma$  oscillations by a single membrane current.

### Mechanisms of $\gamma$ and $\theta$ oscillations in FSI networks

Our model FSI network produces qualitatively different dynamics at high and baseline levels of DA conditions. Under high dopaminergic tone, the FSI network produces high  $\gamma$  band (70 Hz) oscillations modulated by a  $\theta$  (4-6 Hz) oscillation, while under low dopaminergic tone the FSI network produces low  $\gamma$  band (55 Hz) oscillations alone (Fig. 4). While both  $\theta$  and  $\gamma$  are present at the level of individual cells, only in the high DA condition is bursting sufficiently synchronized that  $\theta$  power is present in the network. The presence of  $\theta$  at the network level can be attributed to the higher level of gap junction conductance in the high DA condition (Fig. 3Cii).

The ability of gap junctions to generate synchrony is well established in computational work [29]. Previous models from other groups suggest that gap junctions can enable synchronous bursting in interneurons, such that the burst envelopes are aligned, as in our model [14]. While a shunting effect of low conductance gap junctions can inhibit spiking [30], gap junctions with high enough conductances have an excitatory effect, promoting network synchrony [31,32]. Previous work has also shown the importance of gap junction connectivity in stabilizing network  $\gamma$  oscillations *in silico* [33], as well as network  $\gamma$  and  $\theta$  oscillations in inhibitory networks *in vitro* and *in silico* containing noise or heterogeneity [32]. FSIs *in vivo* are highly connected by gap junctions as well as inhibitory synapses, [34] similar to the networks of inhibitory interneurons that produce ING rhythms [35]. Unlike ING, however, our FSI network  $\gamma$

is independent of GABAergic synapses: inhibitory conductance has only a small impact on  $\gamma$  frequency, and  $\gamma$  power is highest when inhibitory synapses are removed (Figure 3B). In slice, the  $\gamma$  resonance of striatal FSIs is dependent on gap junctions but not on GABA [36], suggesting that our model is an accurate representation of FSI  $\gamma$ .

It is important to note that while our model is conceived as a representation of the dorsal striatal circuit, physiologically similar fast-spiking interneuron networks are present in cortex [10]; therefore, the mechanisms described here may contribute to the generation of  $\theta$ -modulated  $\gamma$  oscillations in cortex as well.

## Support for striatal rhythm generation

Our model provides mechanistic explanations for all four oscillatory bands observed in ventral striatum *in vivo* ( $\theta$ ,  $\beta$ , low  $\gamma$ , and high  $\gamma$ ) [37]. Previous modeling and experiments suggest  $\beta$  can be generated by striatal SPNs [15,38,39]. Our results suggest that FSIs generate striatal  $\gamma$ , and that motor- and reward-related increases in  $\gamma$  power reflect increased striatal FSI activity.

There is evidence to support the existence of a locally generated striatal  $\gamma$  oscillation that is not volume conducted and that responds to local DAergic tone [40,41]. The FSIs of the striatum are the most likely candidate generator of this rhythm: they are unique among striatal cell types in preferentially entraining to periodic input (from each other and from cortex) at  $\gamma$  frequencies [42–46]. Different populations of striatal FSIs *in vivo* entrain to different  $\gamma$  frequencies, and FSIs entrained to higher frequencies are also more entrained to cortical input [25–28]. It is likely that different subpopulations of FSIs selectively entrain to specific  $\gamma$  frequencies depending on physiological differences, context, and neuromodulatory (e.g. DAergic) states; the frequency of  $\gamma$  may itself determine cell assembly size and membership [33].

Experimental evidence also supports striatal FSI involvement in a DA-modulated  $\theta$  rhythm. FSIs phase lock to spontaneous striatal LFP oscillations at  $\theta$  as well as  $\gamma$  frequencies [23,47–51]. *In vivo*, striatal  $\theta$  power is modulated by task-related phenomena such as choice points and motor execution, as well as by reward and reward expectation, suggesting its responsiveness to DA (known to phasically increase in response to reward cues) [4,52–54].  $\theta$  has also been shown to modulate the response of SPNs to reward [55].

## $\theta$ rhythmicity in striatal dynamics and movement

277

*In vivo*, striatal  $\beta$  power has a well established negative correlation with DA and locomotion in both health and disease, while striatal  $\gamma$  power has a positive correlation with both [1,3–6,56].  $\beta$  oscillations in the basal ganglia are thought to provide a “stay” or “status quo” signal that supports maintenance of the currently active motor program [16], and they are causally implicated in motor slowing and cessation [8,56–60].

278

279

280

281

282

In our simulations of high DAergic tone, FSI spiking at high  $\gamma$  frequencies  $\theta$ -periodically inhibits SPN-generated  $\beta$  oscillations, permitting SPN  $\beta$  only during the 150-200 millisecond  $\theta$  trough corresponding to the FSIs’ interburst interval. We hypothesize that these periodic gaps between SPN  $\beta$  packets are necessary to terminate ongoing motor programs and initiate new motor programs, as represented by active SPN assemblies. During the  $\theta$  trough, all SPN cell assemblies are simultaneously released from inhibition and viable to compete once again to determine the current motor program, with incoming input from cortex influencing this competition. Under this interpretation, our results predict that striatal networks oscillate between a “stay” or “program on” state marked by SPN  $\beta$  oscillations, and a “switch” or “program off” state marked by FSI high  $\gamma$  oscillations, and that the  $\theta$  period limits the speed of sequential motor program execution (Fig. 6E).

283

284

285

286

287

288

289

290

291

292

293

294

In support of this hypothesis, striatal representations of behavioral “syllables” that can be combined to create motor programs are active for a maximum of  $\sim 200$  ms [61], and the velocity of continuous motion is modulated intermittently at a  $\theta$  frequency ( $\sim 6-9$  Hz) [62]. In healthy animals, the duration of  $\beta$  bursts has an upper limit of  $\sim 120$  ms, about half a  $\theta$  cycle [8], in agreement with our hypothesis of  $\theta$  phase-modulation of  $\beta$  activity. Striatal  $\gamma$  has also been observed in transient ( $\sim 150$  ms) bursts that are associated with the initiation and vigor of movement [63]. Additionally, other biophysically constrained computational models have suggested that SPN assemblies fire in sequential coherent episodes for durations of several hundred milliseconds, on the timescale of one or several  $\theta$  cycles [64]. Overall, evidence supports the hypothesis that  $\beta$  and  $\gamma$  oscillations in striatum *in vivo*, and therefore the motor states they encode, are activated on  $\theta$ -periodic timescales.

295

296

297

298

299

300

301

302

303

304

305

306

Furthermore,  $\beta$  and  $\gamma$  power are anticorrelated in EEG and corticostriatal

307

LFP [6, 7, 65], in agreement with our model's prediction that these rhythms are coupled 308  
to opposite phases of ongoing  $\theta$  rhythms. FSI and SPN firing are inversely correlated *in* 309  
*vivo*, entrained to  $\theta$ , and they are active during opposite phases of  $\theta$ , as observed in our 310  
model [23, 48, 66–68].  $\theta$ - $\gamma$  cross-frequency coupling is observed in striatum and increases 311  
during reward, when DAergic tone is expected to be high [7, 69–72]. Our model suggests 312  
that these cross-frequency relationships occur in part due to FSI inhibition of SPNs. 313  
Though FSIs are smaller in number, FSI-SPN synapses have a much stronger effect 314  
than SPN-SPN connections, with each FSI inhibiting many SPNs [22, 73]. 315

During baseline DAergic tone in our model, FSIs produce an ongoing low  $\gamma$  that 316  
does not effectively suppress SPN  $\beta$  activity (produced sporadically in both D1 and D2 317  
SPN networks), and thus does not facilitate the switching of the active SPN assembly. 318  
Thus, our model suggests that at baseline levels of DA, switching between SPN 319  
assemblies may be more dependent on cortical inputs or downstream BG circuit 320  
computations. Although the function of FSI low  $\gamma$  inhibition of SPN dynamics is 321  
unclear, it may facilitate striatal responsivity to cortical low  $\gamma$  input, which occurs in an 322  
afferent- and task-specific manner [37]. SPNs do not entrain to  $\gamma$  in our model, 323  
suggesting that  $\gamma$  oscillations are not transmitted to downstream BG structures. 324

In contrast, both the  $\beta$  and  $\theta$  rhythms in our model entrain SPN networks and may 325  
be relayed to other basal ganglia structures. Intriguingly, alternation between  $\beta$  and  $\gamma$  326  
on a  $\theta/\delta$  timescale has been observed in the globus pallidus *in vivo*, and DAergic tone 327  
modulates these oscillations and their interactions [7, 74]. Thus, the mechanisms 328  
proposed in our model may also play a role in the oscillatory dynamics of other basal 329  
ganglia structures, through a combination of rhythm propagation and local rhythm 330  
generation by similar circuits. Similar pauses in FSI activity, allowing transient SPN 331  
disinhibition and production of  $\beta$  oscillations, occur in a recent computational model of 332  
GPe [19], also based on an earlier model of stuttering FSIs [10]. In contrast to this work, 333  
we emphasize the mechanisms producing  $\beta$  and the coordination of  $\beta$  and  $\gamma$  by  $\theta$ , not 334  
addressed previously [19]. 335

## Implications for disease

In Parkinson's disease, which is characterized by motor deficits and chronic DA depletion,  $\beta$  power is correlated with the severity of bradykinesia [1]. Parkinsonian  $\beta$  may be generated by striatal D2 SPNs [15, 38, 39]. Parkinsonian conditions also produce high cholinergic tone [75], known to decrease the conductance of GABAergic FSI-SPN synapses [76]. Thus, the failure of the FSI inhibition-mediated motor program switching described above may play a role in the motor deficits observed in Parkinson's: if DA is low, and FSIs are unable to inhibit either D1 or D2 SPNs,  $\theta$  modulation of SPN  $\beta$  rhythmicity will be supplanted by ongoing D2  $\beta$  rhythmicity, impairing motor initiation by reducing the possibility of motor program switching in the Parkinsonian striatum.

In hyperkinetic motor disorders,  $\gamma$  and  $\theta$  rhythms are potentiated: a mouse model of Huntington's disease (HD) displays unusually high  $\theta$  and  $\gamma$  band striatal LFP power [77–79]; and L-DOPA-induced hyperkinetic dyskinesia is also characterized by increased high  $\gamma$  and  $\theta$  power and reduced  $\beta$  power in the striatal LFP [80–83]. As these rhythms are tied to FSI activation in our model, we suggest that hyperkinetic disorders may result from striatal FSI hyperfunction. Consistent with this hypothesis, in HD model animals, FSI to SPN connectivity is increased, and SPNs respond more strongly to FSI stimulation [84].

However, hypofunction of striatal FSI networks can also lead to hyperkinetic disorders, including Tourette's syndrome, dystonia, and dyskinesias [81–83, 85–88]. Dystonia, which as a disorder of involuntary muscle activation is considered hyperkinetic, can also be characterized by rigidity and freezing due to activation of antagonistic muscles. Indeed, dystonia is characterized by an increase in SPN firing rate due to D2 receptor dysfunction. Our model suggests that FSI hypofunction may be to blame, resulting in excessive SPN  $\beta$  rhythmicity and decreased probability of motor program switching [89]. A reduction in  $\theta/\gamma$  cross frequency coupling has been reported in L-DOPA-induced dyskinesia, suggesting that a chronic hyperkinetic high-DA state may also abolish the FSI-generated  $\theta$ -coupled  $\gamma$  produced here, possibly by pushing the FSI out of its bursting regime and into a tonic spiking mode [90]. These findings underscore the importance of balanced FSI inhibition of SPNs, exemplified by the periodic suppression observed in our model, which we suggest enables the flexible

striatal network activity that allows for smooth, purposeful movements. 367

## Caveats and limitations 368

Little experimental evidence on the striatal FSI D-current conductance exists. The level 369  
of D-current conductance we've chosen leads to  $\gamma$  frequencies and FSI firing rates that 370  
are more in line with experimental observations than previous models. This level of 371  
D-current also produces  $\theta$  rhythmicity in FSI networks. Our parameter choices result in 372  
a model exhibiting a transition between “low DA” and “high DA” dynamic states that 373  
matches experimental observations and has powerful functional interpretations. 374  
Validating our results will require further experimental investigation of the D-current in 375  
striatal FSIs. Interestingly, DA has been shown to downregulate D-current conductance 376  
in prefrontal cortical FSIs. If striatal FSIs exhibited a similar DA-dependent D-current 377  
downregulation, our simulations suggest that the transition between high and low DA 378  
states could be different from that described in the current study. The existence and 379  
functional interpretations of other dynamic transitions are beyond the scope of this 380  
paper. 381

In general, many DA-dependent changes in striatal neurophysiology have been 382  
observed. For the sake of simplicity, most of these have been left out of our modeling. 383  
For example, D1 and D2 SPNs respond differently to adenosine [91] and peptide 384  
release [92], but we did not consider these significant factors in the production of 385  
striatal  $\beta$  oscillations. 386

We also omitted inhibitory connections between D1 and D2 SPN populations. The 387  
connectivity from D1 to D2 SPNs is very sparse (6 percent). Connections from D2 to 388  
D1 SPNs are more prevalent, but it seems unlikely that these projections would 389  
qualitatively alter our results: during the baseline state, the D1 and D2 SPNs are 390  
identical; during the high DA state, SPN inhibition tends to increase SPN  $\beta$  391  
rhythmicity and spiking. 392

In our model the number of FSIs is small, so every FSI participates on every  $\theta$  cycle; 393  
*in vivo*, the participation of multiple FSI populations is likely coordinated by cortex. 394  
Coordinated FSI activity has proven hard to observe over long periods *in vivo* [28, 93]. 395  
However, FSIs form local functional circuits [94], and *in vivo*, striatal FSI assemblies 396



exhibit transient gap-junction dependent synchronization [95], possibly resulting from 397  
brief bouts of correlated cortical or homogeneous DAergic input. Furthermore, different 398  
subpopulations of FSIs have strong preferences for projecting to either D1 or D2 SPNs, 399  
as opposed to the overlapping projections modeled in our current study, and these 400  
distinct populations respond differently to cortical oscillations [49]. Thus, local  $\gamma$  401  
synchrony may exist in small striatal subnetworks and be amplified by DA or cortical 402  
input via the recruitment of multiple FSI subpopulations. 403

Finally, cortical input to both FSIs and SPNs was simulated as Poisson noise. In a 404  
sense, then, we simulated a model of striatum to which cortex is not providing 405  
informative input. It could be the case that this is a population that is not “selected” 406  
by cortex to take part in motor activity, a population that is in a “listening” state 407  
awaiting cortical input, or a population taking part in a learned behavior that can be 408  
executed without cortical input. However, cortical input is probably essential in 409  
determining which SPNs and FSIs take part in network oscillatory activity. If the FSIs 410  
play a role in organizing the response of the SPNs to cortical input, changing the 411  
properties of the simulated input may prove informative in terms of how this 412  
organization might take place. In particular, cortical inputs may be more correlated 413  
within certain FSI subpopulations than others. Previous modeling work has shown that 414  
networks of striatal FSIs can detect correlated input [30], a property that may play an 415  
important computational role in striatal function. Additionally, we can expect that 416  
input from cortex has oscillatory properties of its own. Exploring these complexities is 417  
an important direction for future research into the role of striatal GABAergic networks 418  
and rhythmic dynamics in motor behavior. 419

## Materials and methods 420

All neurons (FSIs and SPNs) are modeled using conductance-based models with 421  
Hodgkin-Huxley-type dynamics. SPNs are modeled with a single compartment and FSIs 422  
have two compartments to represent the soma and a dendrite. The temporal voltage 423  
change of each neuron is described by (Eqn. 1): 424

$$c_m \frac{dV}{dt} = - \sum I_{memb} - \sum I_{syn} + I_{app} \quad (1)$$

Membrane voltage ( $V$ ) has units of  $mV$ . Currents have units of  $\mu A/cm^2$ . The specific membrane capacitance ( $c_m$ ) is  $1 mF/cm^2$  for all FSIs and SPNs. Each model neuron has intrinsic membrane currents ( $I_{memb}$ ) and networks of neurons include synaptic currents ( $I_{syn}$ ). The applied current term ( $I_{app}$ ) represents background excitation to an individual neuron and is the sum of a constant and a noise term.

All membrane currents have Hodgkin-Huxley-type conductances formulated as:

$$I = \bar{g}(m^n h^k)(V - E_{ion}) \quad (2)$$

Each current in Eqn.2 has a constant maximal conductance ( $\bar{g}$ ) and a constant reversal potential ( $E_{ion}$ ). The activation ( $m$ ) and inactivation ( $h$ ) gating variables have  $n^{th}$  and  $k^{th}$  order kinetics, where  $n, k \geq 0$ . The dynamics of each gating variable evolves according to the kinetic equation (written here for the gating variable  $m$ ):

$$\frac{dm}{dt} = \frac{m_\infty - m}{\tau_m} \quad (3)$$

The steady-state functions ( $m_\infty$ ) and the time constant of decay ( $\tau_m$ ) can be formulated using the rate functions for opening ( $\alpha_m$ ) and closing ( $\beta_m$ ) of the ionic channel by using the equations:

$$m_\infty = \alpha_m / (\alpha_m + \beta_m)$$
$$\tau_m = 1 / (\alpha_m + \beta_m).$$

The specific functions and constants for different cell types are given below.

## Striatal fast spiking interneurons

Striatal fast spiking interneurons (FSIs) were modeled as in Golomb et al., 2007 [10] using two compartments. The voltage in the somatic compartment ( $V$ ) and in the dendrite ( $V_d$ ) evolve according to:

$$c_m \frac{dV}{dt} = -I_{Na} - I_K - I_L - I_D - I_{syn} \quad (4)$$

$$c_m \frac{dV_d}{dt} = -I_{Na} - I_K - I_L - I_D - I_{syn} + I_{ext} \quad (5)$$

Background excitation is represented by the term  $I_{ext}$ , which is formulated as the sum of a tonic, DA dependent current and Poisson input. The units of  $I_{ext}$  are in  $\mu A/cm^2$ . The tonic, DA dependent current is discussed below. Each FSI receives independent, excitatory Poisson input with a rate of 2000 inputs per second.

The synaptic current ( $I_{syn}$ ) is the sum of GABA<sub>A</sub> currents and electrical connections between FSIs (formulated below). The FSI membrane currents ( $I_{memb}$ ) consisted of a fast sodium current ( $I_{Na}$ ), a fast potassium current ( $I_k$ ), a leak current ( $I_L$ ), and a D-current ( $I_D$ ). The formulations of these currents were taken from previous models of striatal FSIs. [10,17]

The maximal sodium conductance is  $\bar{g}_{Na} = 112mS$  and the sodium reversal potential is  $E_{Na} = 50mV$ . The sodium current has three activation gates ( $n = 3$ ) and one inactivation gate ( $k = 1$ ). The steady state functions for the sodium current activation ( $m$ ) and inactivation ( $h$ ) variables and their time constants ( $\tau_m$  and  $\tau_h$ , respectively) are described by:

$$m_\infty = \frac{1}{1 + \exp[-(V + 24)/11.5]} \quad (6)$$

$$h_\infty = \frac{1}{1 + \exp[(V + 58.3)/6.7]} \quad (7)$$

$$\tau_h = 0.5 + \frac{14}{1 + \exp[(V + 60)/12]} \quad (8)$$

The maximal conductance for the fast potassium channel is  $\bar{g}_K = 225mS$  and the reversal potential for potassium is  $E_K = -90mV$ . The fast potassium channel has no inactivation gates but has four activation gates described by its steady state function ( $n_\infty$ ) and time constant ( $\tau_n$ ):

$$n_\infty = \frac{1}{1 + \exp[-(V + 12.4)/6.8]} \quad (9)$$

$$\tau_n = \left(0.087 + \frac{11.4}{1 + \exp[(V + 14.6)/8.6]}\right) \left(0.087 + \frac{11.4}{1 + \exp[-(V - 1.3)/18.7]}\right) \quad (10)$$

The leak current ( $I_L$ ) has no gating variables. The maximal leak channel conductance is  $g_L = 0.25mS$  and the leak channel reversal potential is  $E_L = -70mV$ .

The D-current ( $I_D$ ) is described mathematically as in Golomb et al, 2007 [10] and has one activation (a) and one inactivation (b) gate. The steady state functions for the activation and inactivation gates are formulated as:

$$a_\infty = \frac{1}{1 + \exp[-(V + 50)/20]} \quad (11)$$

$$b_\infty = \frac{1}{1 + \exp[(V + 70)/6]} \quad (12)$$

The time constant of the decay is 2 ms ( $\tau_a$ ) for the activation gate and 150 ms ( $\tau_b$ ) for the inactivation gate. The maximal conductance of the D-current is 6 mS.

## Striatal spiny projection neurons

Spiny projection neurons were modeled with four membrane currents: a fast sodium current ( $I_{Na}$ ), a fast potassium current ( $I_k$ ), a leak current ( $I_L$ ), and an M-current ( $I_m$ ) [11]. We do not model SPN up and down states which are not prevalent in the awake state of striatum [96], the state being modeled, and therefore we do not include the Kir current in our model, which is active during the SPN down state.

The sum of all excitatory inputs from the cortex and thalamus and inhibitory inputs from striatal interneurons is introduced into the model using a background excitation term ( $I_{app}$ ).  $I_{app}$  is the sum of a constant term and a Gaussian noise term. The Gaussian noise has mean zero, standard deviation one and an amplitude of  $4\sqrt{\delta t}$  where  $\delta t$  is the time step of integration. D1 and D2 SPNs were distinguished only by the value of tonic term of  $I_{app}$  when DA levels were high. DA is excitatory to D1 receptors and inhibitory to D2 receptors [97]. Thus, we modeled D1 and D2 SPNs as having the same tonic  $I_{app}$  at baseline DAergic tone state with  $I_{app} = 1.19\mu A/cm^2$ . To model the high DA state, let the tonic term of  $I_{app} = 2.19\mu A/cm^2$  for the D1 SPNs and  $I_{app} = 0.19\mu A/cm^2$  for the D2 SPNs.

*Fast sodium current:* The rate functions for the sodium current activation ( $m$ ) and inactivation ( $h$ ) variables are formulated as:

$$\alpha_m = \frac{0.32(V + 54)}{1 - \exp[-(V + 54)/4]} \quad (13)$$

$$\beta_m = \frac{0.28(V + 27)}{\exp[(V + 27)/5] - 1} \quad (14)$$

$$\alpha_h = 0.128 \exp[-(V + 50)/18] \quad (15)$$

$$\beta_h = \frac{4}{1 + \exp[-(V + 27)/5]} \quad (16)$$

The maximal conductance of the sodium current is  $\bar{g}_{Na} = 100mS$ . The sodium reversal potential is  $E_{Na} = 50mV$ . The sodium current has three activation gates ( $n = 3$ ) and only one inactivation gate ( $k = 1$ ).

*Fast potassium current:* The fast potassium current ( $I_K$ ) has four activation gates ( $n = 4$ ) and no inactivation gates ( $k = 0$ ). The rate functions of the activation gate are described by:

$$\alpha_m = \frac{0.032(V + 52)}{1 - \exp[-(V + 52)/5]} \quad (17)$$

$$\beta_m = 0.5 \exp[-(V + 57)/40] \quad (18)$$

The maximal fast potassium channel conductance is  $\bar{g}_K = 80mS$ . The reversal potential for potassium is  $E_K = -100mV$ .

*Leak Current:* The leak current ( $I_L$ ) has no gating variables ( $n = 0, k = 0$ ). The maximal conductance of the leak channel is  $g_L = 0.1mS$ . The leak channel reversal potential is  $E_L = -67mV$ .

*M-current:* The M-current has one activation gate ( $n = 1$ ) and no inactivation gate ( $k = 0$ ). The rate functions for the M-current activation gate are described by:

$$\alpha_m = \frac{Q_s 10^{-4}(V + 30)}{1 - \exp[-(V + 30)/9]} \quad (19)$$

$$\beta_m = -\frac{Q_s 10^{-4}(V + 30)}{1 - \exp[(V + 30)/9]} \quad (20)$$

We use a  $Q_{10}$  factor of 2.3 to scale the rate functions of the M-current since the original formulation of these kinetics described dynamics at 23 °C [98]. Thus, for a normal body temperature of 37 °C, the M-current rate equations are scaled by  $Q_s$ ,

which is formulated as:

$$Q_s = Q_{10}^{(37^\circ\text{C}-23^\circ\text{C})/10} = 3.209 \quad (21)$$

The maximal M-current conductance is  $\bar{g}_m = 1.29mS$ .

## Synaptic connectivity and networks

Networks of FSIs contained 100 neurons. For networks that additionally had SPNs, we modeled 100 D1 SPNs and 100 D2 SPNs. Due to computational constraints, we did not include enough SPNs to simulate a realistic ratio of interneurons to projection neurons. Although in rodents, interneurons consist of at most 5% of all cells in the striatum [9], interneurons account for at least 25% of neurons in the human striatum [99]. Thus, our networks consist of proportions of FSIs and SPNs that are likely closer to those found in humans than rodents.

The model synaptic GABA<sub>A</sub> current ( $I_{\text{GABA}_A}$ ) is formulated as in McCarthy et al., 2011 [15] and is the only synaptic connection between SPNs and from FSIs to SPNs. The GABA<sub>A</sub> current has a single activation gate dependent on the pre-synaptic voltage.

$$I_{\text{GABA}_A} = \bar{g}_{ii} s_i (V - E_i) \quad (22)$$

The maximal GABA<sub>A</sub> conductance between FSIs is  $\bar{g}_{ii} = 0.08mS$ . The maximal GABA<sub>A</sub> conductance from FSIs to SPNs is  $\bar{g}_{ii} = 0.6mS$  and between SPNs was  $\bar{g}_{ii} = 0.1mS$ . These values are consistent with FSI to SPN inhibition being approximately six times stronger than inhibition between SPNs [9].

The gating variable for inhibitory GABA<sub>A</sub> synaptic transmission is represented by  $s_i$ . For the  $j^{\text{th}}$  neuron (FSI or SPN) in the network:

$$s_j = \sum_{k=1}^N S_{i_k i_j} \quad (23)$$

The variable  $S_{i_k i_j}$  describes the kinetics of the gating variable from the  $k^{\text{th}}$  pre-synaptic neuron to the  $j^{\text{th}}$  post-synaptic neuron. This variable evolves in time according to:

$$\frac{dS_{i_k i_j}}{dt} = g_{\text{GABA}_A}(V_k)(1 - S_{i_k i_j}) - \frac{S_{i_k i_j}}{\tau_i} \quad (24)$$

The GABA<sub>A</sub> time constant of decay ( $\tau_i$ ) is set to 13 ms for SPN to SPN connections [97] as well as for FSI to FSI connections and FSI to SPN connections [30]. The GABA<sub>A</sub> current reversal potential ( $E_i$ ) for both FSIs and SPNs is set to -80 mV. The rate functions for the open state of the GABA<sub>A</sub> receptor ( $g_{\text{GABA}_A}(V_k)$ ) for SPN to SPN transmission is described by:

$$g_{\text{GABA}_A}(V_k) = 2(1 + \tanh(\frac{V_k}{4})) \quad (25)$$

The rate functions for the open state of the GABA<sub>A</sub> receptor ( $g_{\text{GABA}_A}(V_k)$ ) for FSI to FSI and FSI to SPN transmission is:

$$g_{\text{GABA}_A}(V_k) = \frac{1}{\tau_r}(1 + \tanh(\frac{V_k}{10})) \quad (26)$$

The value of  $\tau_r$  is 0.25 ms. FSIs were additionally connected by dendritic electrical connections. The electrical coupling for dendritic compartment  $i$  is denoted as  $I_{elec}$ , has units in  $\mu A/cm^2$  and is formulated as:

$$I_{elec} = g_{\text{gap}}(Vd_j - Vd_i) \quad (27)$$

The value of the gap junction conductance  $g_{\text{gap}}$  depended on DA level (see below). Within the 100-cell FSI network, each pair of FSIs had an independent 30 percent chance of a dendro-dendritic gap junction chosen from a uniform random distribution and an independent 30 percent chance of a somato-somatic inhibitory synapse also chosen from a uniform distribution. SPNs are connected with each other in a mutually inhibitory GABAergic network [100]. We modeled all to all connectivity of inhibitory synapses from any SPN to any SPN of the same receptor subtype.

## DA

DA impacts both connectivity and excitability in the model networks. DAergic tone was simulated as having five components: direct excitation of FSIs [12], increased gap

junction conductance between FSIs [13], decreased inhibitory conductance between FSIs [12], increased excitation to D1 SPNs, and decreased excitation to D2 SPNs. DA-induced changes to SPN excitation were discussed above. Excitation to FSIs was modeled as the sum of a tonic, DA dependent input current ( $I_{tonic}$ ) and a noise term. DA did not change the noise term in either SPNs or FSIs. The baseline DAergic tone state was modeled in FSIs using  $I_{tonic} = 4\mu A/cm^2$ ,  $g_{gap} = 0.05mS$  and the GABA<sub>A</sub> conductance between FSIs was  $g_{ii} = 0.1mS$ . The high DA state was modeled in FSIs using  $I_{tonic} = 14\mu A/cm^2$ ,  $g_{gap} = 0.2mS$  and  $g_{ii} = 0.005mS$ .

## Local field potential

The local field potential (LFP) was calculated as the sum of all voltages in all cells. Stationarity of the network appears in the raster plots after about 500 ms. To eliminate transients due to initial conditions, our LFP is evaluated only after 1,000 ms of simulated time. We estimated the power spectral density of the simulated LFP using the multitaper method [101].

## Simulations

All simulations were run on the MATLAB-based programming platform DynaSim, a framework for efficiently developing, running and analyzing large systems of coupled ordinary differential equations, and evaluating their dynamics over large regions of parameter space [102]. DynaSim is open-source and all models have been made publicly available using this platform. All differential equations were integrated using a fourth-order Runge-Kutta algorithm with time step was .01 ms. Plotting and analysis were performed with inbuilt and custom MATLAB code.

## Acknowledgments

We thank Jason Sherfey and Erik Roberts for developing the DynaSim Toolbox used to run the simulations in this manuscript and assisting with debugging and visualization. In addition, we thank Sean Patrick for assistance in interpreting the behavioral implications of our model.



## References

1. BROWN P, WILLIAMS D. Basal ganglia local field potential activity: Character and functional significance in the human. *Clinical Neurophysiology*. 2005;116(11):2510–2519.
2. Berke JD. Fast oscillations in cortical-striatal networks switch frequency following rewarding events and stimulant drugs. *European Journal of Neuroscience*. 2009;30(5):848–859.
3. Stenner MP, Dürschmid S, Rutledge RB, Zaehle T, Schmitt FC, Kaufmann J, et al. Perimovement decrease of alpha/beta oscillations in the human nucleus accumbens. *Journal of Neurophysiology*. 2016;116(4):1663–1672.
4. Doñamayor N, Schoenfeld MA, Münte TF. Magneto- and electroencephalographic manifestations of reward anticipation and delivery. *NeuroImage*. 2012;62(1):17–29.
5. Jenkinson N, Brown P. New insights into the relationship between dopamine, beta oscillations and motor function. *Trends in Neurosciences*. 2011;34(12):611–618.
6. Jenkinson N, Kühn Aa, Brown P. Gamma oscillations in the human basal ganglia. *Experimental Neurology*. 2013;245:72–76.
7. López-Azcárate J, Nicolás MJ, Cordon I, Alegre M, Valencia M, Artieda J. Delta-mediated cross-frequency coupling organizes oscillatory activity across the rat cortico-basal ganglia network. *Frontiers in neural circuits*. 2013;7(October):1–16.
8. Feingold J, Gibson DJ, DePasquale B, Graybiel AM. Bursts of beta oscillation differentiate postperformance activity in the striatum and motor cortex of monkeys performing movement tasks. *Proceedings of the National Academy of Sciences*. 2015;112(44):13687–13692.
9. Koos T, Tepper JM, Wilson CJ. Comparison of IPSCs Evoked by Spiny and Fast-Spiking Neurons in the Neostriatum. *Journal of Neuroscience*. 2004;24(36):7916–7922.

10. Golomb D, Donner K, Shacham L, Shlosberg D, Amitai Y, Hansel D. Mechanisms of firing patterns in fast-spiking cortical interneurons. *PLoS Computational Biology*. 2007;3(8):1498–1512.
11. Shen W. Cholinergic Suppression of KCNQ Channel Currents Enhances Excitability of Striatal Medium Spiny Neurons. *Journal of Neuroscience*. 2005;25(32):7449–7458.
12. Bracci E, Vreugdenhil M, Hack SP, Jefferys JGR. Dynamic Modulation of Excitation and Inhibition During Stimulation at Gamma and Beta Frequencies in the CA1 Hippocampal Region. *Journal of Neurophysiology*. 2001;85(6):2412–2422.
13. Onn SP, Grace AA. Dye coupling between rat striatal neurons recorded in vivo: compartmental organization and modulation by dopamine. <https://doi.org/10.1152/jn.1994.71.5.1917>. 1994;.
14. Skinner FK, Zhang L, Velazquez JLP, Carlen PL. Bursting in Inhibitory Interneuronal Networks : A Role for Gap-Junctional Coupling. *Journal of Neurophysiology*. 1999;81(3):1274–1283.
15. McCarthy MM, Moore-Kochlacs C, Gu X, Boyden ES, Han X, Kopell N. Striatal origin of the pathologic beta oscillations in Parkinson’s disease. *Proceedings of the National Academy of Sciences of the United States of America*. 2011;108(28):11620–11625.
16. Engel AK, Fries P. Beta-band oscillations—signalling the status quo? *Current opinion in neurobiology*. 2010;20(2):156–165.
17. Sciamanna G, Wilson CJ. The ionic mechanism of gamma resonance in rat striatal fast-spiking neurons. *Journal of Neurophysiology*. 2011;106(6):2936–2949.
18. Lewis TJ, Rinzel J. Dendritic effects in networks of electrically coupled fast-spiking interneurons. *Neurocomputing*. 2004;58-60:145 – 150. doi:<https://doi.org/10.1016/j.neucom.2004.01.035>.

19. Corbit VL, Whalen TC, Zitelli KT, Crilly SY, Rubin JE, Gittis AH. Pallidostriatal Projections Promote Oscillations in a Dopamine-Depleted Biophysical Network Model. *Journal of Neuroscience*. 2016;36(20):5556–5571.
20. Schultz W, Dayan P, Montague PR. A neural substrate of prediction and reward. *Science (New York, NY)*. 1997;275(5306):1593–9. doi:10.1126/SCIENCE.275.5306.1593.
21. Chow CC, White JA, Ritt J, Kopell N. Frequency Control in Synchronized Networks of Inhibitory Neurons. *Journal of Computational Neuroscience*. 1998;5(4):407–420. doi:10.1023/A:1008889328787.
22. Koós T, Tepper JM. Inhibitory control of neostriatal projection neurons by GABAergic interneurons. *Nature neuroscience*. 1999;2(5):467–72.
23. Berke JD, Breck JT, Eichenbaum H. Striatal Versus Hippocampal Representations During Win-Stay Maze Performance. *Journal of Neurophysiology*. 2009;101(3):1575–1587.
24. Bracci E, Centonze D, Bernardi G, Calabresi P. Voltage-dependent membrane potential oscillations of rat striatal fast-spiking interneurons. *The Journal of Physiology*. 2003;549(1):121–130.
25. van der Meer Maa, Kalenscher T, Lansink CS, Pennartz CMA, Berke JD, Redish aD. Integrating early results on ventral striatal gamma oscillations in the rat. *Frontiers in Neuroscience*. 2010;4(SEP):1–12.
26. van der Meer MAAA, Redish AD. Low and High Gamma Oscillations in Rat Ventral Striatum have Distinct Relationships to Behavior, Reward, and Spiking Activity on a Learned Spatial Decision Task. *Frontiers in integrative neuroscience*. 2009;3(June):9.
27. Catanese J, Carmichael JE, van der Meer MAA. Low- and high-gamma oscillations deviate in opposite directions from zero-phase synchrony in the limbic corticostriatal loop. *Journal of Neurophysiology*. 2016;116(1):5–17.

28. Kalenscher T, Lansink CS, Lankelma JV, Pennartz CMA. Reward-associated gamma oscillations in ventral striatum are regionally differentiated and modulate local firing activity. *Journal of neurophysiology*. 2010;103(3):1658–1672.
29. Sherman A, Rinzel J, Keizer J. Emergence of organized bursting in clusters of pancreatic beta-cells by channel sharing. *Biophysical Journal*. 1988;54(3):411–425. doi:10.1016/S0006-3495(88)82975-8.
30. Hjorth J, Blackwell KT, Kotaleski JH. Gap junctions between striatal fast-spiking interneurons regulate spiking activity and synchronization as a function of cortical activity. *The Journal of neuroscience : the official journal of the Society for Neuroscience*. 2009;29(16):5276–5286.
31. Munro E, Börgers C. Mechanisms of very fast oscillations in networks of axons coupled by gap junctions. *Journal of Computational Neuroscience*. 2010;28(3):539–555. doi:10.1007/s10827-010-0235-6.
32. Traub RD, Kopell N, Bibbig a, Buhl EH, LeBeau FE, Whittington Ma. Gap junctions between interneuron dendrites can enhance synchrony of gamma oscillations in distributed networks. *The Journal of neuroscience : the official journal of the Society for Neuroscience*. 2001;21(23):9478–9486.
33. Börgers C, Talei Franzesi G, LeBeau FEN, Boyden ES, Kopell NJ, Franzesi G, et al. Minimal size of cell assemblies coordinated by gamma oscillations. *PLoS Computational Biology*. 2012;8(2):e1002362.
34. Fukuda T. Network Architecture of Gap Junction-Coupled Neuronal Linkage in the Striatum. *Journal of Neuroscience*. 2009;doi:10.1523/jneurosci.4418-08.2009.
35. Whittington Ma, Traub RD, Kopell N, Ermentrout B, Buhl EH. Inhibition-based rhythms: Experimental and mathematical observations on network dynamics. *International Journal of Psychophysiology*. 2000;38:315–336.
36. Russo G, Nieuwenhuis TR, Maggi S, Taverna S. Dynamics of action potential firing in electrically connected striatal fast-spiking interneurons. *Frontiers in cellular neuroscience*. 2013;7(November):209.

37. Berke JD. Functional properties of striatal fast-spiking interneurons. *Frontiers in systems neuroscience*. 2011;5(June):45.
38. Kondabolu K, Roberts EA, Bucklin M, McCarthy MM, Kopell N, Han X. Striatal cholinergic interneurons generate beta and gamma oscillations in the corticostriatal circuit and produce motor deficits. *Proceedings of the National Academy of Sciences*. 2016;113(22):E3159–E3168.
39. Pittman-Polletta BR, Quach A, Mohammed AI, Romano M, Kondabolu K, Kopell NJ, et al. Striatal cholinergic receptor activation causes a rapid, selective, & state-dependent rise in corticostriatal  $\beta$  activity. *European Journal of Neuroscience*. 2018; p. 1–13.
40. Popescu AT, Popa D, Paré D. Coherent gamma oscillations couple the amygdala and striatum during learning. *Nature neuroscience*. 2009;12(6):801–807.
41. West TO, Berthouze L, Halliday DM, Litvak V, Sharott A, Magill PJ, et al. Propagation of Beta/Gamma Rhythms in the Cortico-Basal Ganglia Circuits of the Parkinsonian Rat. *Journal of Neurophysiology*. 2018; p. jn.00629.2017.
42. Surmeier DJJ, Carrillo-Reid L, Bargas J. Dopaminergic modulation of striatal neurons, circuits, and assemblies. *Neuroscience*. 2011;198:3–18.
43. Schulz JM, Pitcher TL, Savanthrapadian S, Wickens JR, Oswald MJ, Reynolds JNJ. Enhanced high-frequency membrane potential fluctuations control spike output in striatal fast-spiking interneurons in vivo. *The Journal of physiology*. 2011;589(17):4365–4381.
44. Belić JJ, Kumar A, Kotaleski JH, Hellgren Kotaleski J. Interplay between periodic stimulation and GABAergic inhibition in striatal network oscillations. *PLoS ONE*. 2017;12(4):e0175135.
45. Beatty JA, Song SC, Wilson CJ. Cell-type-specific resonances shape the responses of striatal neurons to synaptic input. *Journal of Neurophysiology*. 2015;113(3):688–700.

46. Mancilla JG, Lewis TJ, Pinto DJ, Rinzel J, Connors BW. Synchronization of Electrically Coupled Pairs of Inhibitory Interneurons in Neocortex. *Journal of Neuroscience*. 2007;27(8):2058–2073.
47. Sharott A, Moll CKE, Engler G, Denker M, Grun S, Engel AK, et al. Different subtypes of striatal neurons are selectively modulated by cortical oscillations. *The Journal of neuroscience : the official journal of the Society for Neuroscience*. 2009;29(14):4571–4585.
48. Sharott A, Doig NM, Mallet N, Magill PJ. Relationships between the Firing of Identified Striatal Interneurons and Spontaneous and Driven Cortical Activities In Vivo. *Journal of Neuroscience*. 2012;32(38):13221–13236.
49. Garas FN, Shah RS, Kormann E, Doig NM, Vinciati F, Nakamura KC, et al. Secretagogin expression delineates functionally-specialized populations of striatal parvalbumin-containing interneurons. *eLife*. 2016;5(September):e16088.
50. Carmichael JE, Gmaz JM, van der Meer MAA. Gamma Oscillations in the Rat Ventral Striatum Originate in the Piriform Cortex. *The Journal of Neuroscience*. 2017;37(33):7962–7974.
51. Lalla L, Rueda Orozco PE, Jurado-Parras MT, Brovelli A, Robbe D, Rueda-Orozco P, et al. Local or Not Local: Investigating the Nature of Striatal Theta Oscillations in Behaving Rats. *eneuro*. 2017;4(October):ENEURO.0128–17.2017.
52. Lepski G, Arévalo A, do Valle AC, Ballester G, Gharabaghi A. Increased coherence among striatal regions in the theta range during attentive wakefulness. *Brazilian Journal of Medical and Biological Research*. 2012;45(8):763–770.
53. Kimchi EY, Torregrossa MM, Taylor JR, Laubach M. Neuronal correlates of instrumental learning in the dorsal striatum. *Journal of neurophysiology*. 2009;102(1):475–489.
54. DeCoteau WEW, Thorn C, Gibson DJ, Courtemanche R, Mitra P, Kubota Y, et al. Oscillations of local field potentials in the rat dorsal striatum during

- spontaneous and instructed behaviors. *Journal of neurophysiology*. 2007;97(5):3800–3805.
55. van der Meer MAA, Redish AD, Meer MAAVD, Redish AD. Theta Phase Precession in Rat Ventral Striatum Links Place and Reward Information. *Journal of Neuroscience*. 2011;31(8):2843–2854.
  56. Tan H, Wade C, Brown P. Post-Movement Beta Activity in Sensorimotor Cortex Indexes Confidence in the Estimations from Internal Models. *Journal of Neuroscience*. 2016;36(5).
  57. Brown P. Abnormal oscillatory synchronisation in the motor system leads to impaired movement. *Current Opinion in Neurobiology*. 2007;17(6):656–664.
  58. Khanna P, Carmena JM. Beta band oscillations in motor cortex reflect neural population signals that delay movement onset. *eLife*. 2017;6:1–31.
  59. Lemos JC, Friend DM, Kaplan AR, Shin JH, Rubinstein M, Kravitz AV, et al. Enhanced GABA Transmission Drives Bradykinesia Following Loss of Dopamine D2 Receptor Signaling. *Neuron*. 2016;90(4):824–838.
  60. Little S, Brown P. The functional role of beta oscillations in Parkinson’s disease. *Parkinsonism and Related Disorders*. 2014;20(SUPPL.1):S44–S48.
  61. Markowitz JE, Gillis WF, Beron CC, Neufeld SQ, Robertson K, Bhagat ND, et al. The Striatum Organizes 3D Behavior via Moment-to-Moment Action Selection. *Cell*. 2018;174(1):44–58.e17.
  62. Gross J, Timmermann L, Kujala J, Dirks M, Schmitz F, Salmelin R, et al. The neural basis of intermittent motor control in humans. *Proceedings of the National Academy of Sciences of the United States of America*. 2002;99(4):2299–302.
  63. Masimore B, Schmitzer-Torbert NC, Kakalios J, Redish AD. Transient striatal gamma local field potentials signal movement initiation in rats. *Neuroreport*. 2005;16(18):2021–2024.

64. Humphries MD, Wood R, Gurney K. Dopamine-modulated dynamic cell assemblies generated by the GABAergic striatal microcircuit. *Neural Networks*. 2009;22(8):1174–1188.
65. Zhang Y, Pan X, Wang R, Sakagami M. Functional connectivity between prefrontal cortex and striatum estimated by phase locking value. *Cognitive Neurodynamics*. 2016;10(3):245–254.
66. Howe MW, Atallah HE, McCool A, Gibson DJ, Graybiel AM. Habit learning is associated with major shifts in frequencies of oscillatory activity and synchronized spike firing in striatum. *Proceedings of the National Academy of Sciences*. 2011;108(40):16801–16806.
67. Thorn CA, Graybiel AM. Differential Entrainment and Learning-Related Dynamics of Spike and Local Field Potential Activity in the Sensorimotor and Associative Striatum. *Journal of Neuroscience*. 2014;34(8):2845–2859.
68. Berke JD, Okatan M, Skurski J, Eichenbaum HB. Oscillatory entrainment of striatal neurons in freely moving rats. *Neuron*. 2004;43(6):883–896.
69. von Nicolai C, Engler G, Sharott A, Engel AK, Moll CK, Siegel M, et al. Corticostriatal Coordination through Coherent Phase-Amplitude Coupling. *The Journal of neuroscience : the official journal of the Society for Neuroscience*. 2014;34(17):5938–48.
70. Dzirasa K, Coque L, Sidor MM, Kumar S, Dancy EA, Takahashi JS, et al. Lithium Ameliorates Nucleus Accumbens Phase-Signaling Dysfunction in a Genetic Mouse Model of Mania. *Journal of Neuroscience*. 2010;30(48):16314–16323.
71. Cohen MX, Axmacher N, Lenartz D, Elger CE, Sturm V, Schlaepfer TE. Good Vibrations: Cross-frequency Coupling in the Human Nucleus Accumbens during Reward Processing. *Journal of Cognitive Neuroscience*. 2009;21(5):875–889.
72. Tort ABL, Kramer MA, Thorn C, Gibson DJ, Kubota Y, Graybiel AM, et al. Dynamic cross-frequency couplings of local field potential oscillations in rat striatum and hippocampus during performance of a T-maze task. *Proceedings of*



the National Academy of Sciences of the United States of America.

2008;105(51):20517–20522.

73. Tepper JM, Wilson CJ, Koós T. Feedforward and feedback inhibition in neostriatal GABAergic spiny neurons. *Brain Research Reviews*. 2008;58(2):272–281.
74. Dejean C, Arbuthnott G, Wickens JR, Le Moine C, Boraud T, Hyland BI. Power Fluctuations in Beta and Gamma Frequencies in Rat Globus Pallidus: Association with Specific Phases of Slow Oscillations and Differential Modulation by Dopamine D1 and D2 Receptors. *Journal of Neuroscience*. 2011;31(16):6098–6107.
75. Ikarashi Y, Takahashi A, Ishimaru H, Arai T, Maruyama Y. Regulation of Dopamine D1 and D2 Receptors on Striatal Acetylcholine Release in Rats. *Brain Research Bulletin*. 1997;43(1):107–115. doi:10.1016/S0361-9230(96)00351-6.
76. Koós T, Tepper JM. Dual cholinergic control of fast-spiking interneurons in the neostriatum. *The Journal of neuroscience : the official journal of the Society for Neuroscience*. 2002;22(2):529–35. doi:10.1523/JNEUROSCI.22-02-00529.2002.
77. Miller BR, Walker AG, Barton SJ, Rebec GV. Dysregulated Neuronal Activity Patterns Implicate Corticostriatal Circuit Dysfunction in Multiple Rodent Models of Huntington’s Disease. *Frontiers in systems neuroscience*. 2011;5(May):26.
78. Tepper JM, Tecuapetla F, Koós T, Ibáñez-sandoval O, Kreitzer A. Heterogeneity and Diversity of Striatal GABAergic Interneurons. *Frontiers in Neuroanatomy*. 2010;4(December):1–18.
79. Ghiglieri V, Bagetta V, Calabresi P, Picconi B. Functional interactions within striatal microcircuit in animal models of Huntington’s disease. *Neuroscience*. 2012;211:165–184.
80. Alam M, Capelle H, Schwabe K, Krauss JK. Brain Stimulation Effect of Deep Brain Stimulation on Levodopa-Induced Dyskinesias and Striatal Oscillatory

- Local Field Potentials in a Rat Model of Parkinson ' s Disease. *Brain Stimulation*. 2014;7(1):13–20.
81. Gittis AH, Kreitzer AC. Striatal Microcircuitry and Movement Disorders. *Trends in Neurosciences*. 2013;31(9):1713–1723.
82. Reiner A, Shelby E, Wang H, DeMarch Z, Deng Y, Guley NH, et al. Striatal parvalbuminergic neurons are lost in Huntington's disease: implications for dystonia. *Movement Disorders*. 2013;28(12):1691–1699.
83. Rothe T, Deliano M, Wójtowicz AM, Dvorchak A, Harnack D, Paul S, et al. Pathological gamma oscillations, impaired dopamine release, synapse loss and reduced dynamic range of unitary glutamatergic synaptic transmission in the striatum of hypokinetic Q175 Huntington mice. *Neuroscience*. 2015;311:519–538.
84. Cepeda C, Galvan L, Holley SM, Rao SP, André VM, Botelho EP, et al. Multiple sources of striatal inhibition are differentially affected in Huntington's disease mouse models. *The Journal of neuroscience : the official journal of the Society for Neuroscience*. 2013;33(17):7393–406.
85. Gittis AH, Leventhal DK, Fensterheim BA, Pettibone JR, Berke JD, Kreitzer AC. Selective inhibition of striatal fast-spiking interneurons causes dyskinesias. *The Journal of neuroscience : the official journal of the Society for Neuroscience*. 2011;31(44):15727–31.
86. Vinner E, Israelashvili M, Bar-Gad I. Prolonged striatal disinhibition as a chronic animal model of tic disorders. *Journal of Neuroscience Methods*. 2017;292:20–29.
87. Leckman JF, Bloch MH, Smith ME, Larabi D, Hampson M. Neurobiological substrates of Tourette's disorder. *Journal of child and adolescent psychopharmacology*. 2010;20(4):237–47.
88. Xu M, Li L, Pittenger C. Ablation of fast-spiking interneurons in the dorsal striatum, recapitulating abnormalities seen post-mortem in Tourette syndrome, produces anxiety and elevated grooming. *Neuroscience*. 2016;324(2):321–329.

89. Sciamanna G, Bonsi P, Tassone A, Cuomo D, Tschertner A, Viscomi MT, et al. Impaired striatal D2 receptor function leads to enhanced GABA transmission in a mouse model of DYT1 dystonia. *Neurobiology of Disease*. 2009;34(1):133–145.
90. Belić JJ, Halje P, Richter U, Petersson P, Hellgren Kotaleski J. Untangling Cortico-Striatal Connectivity and Cross-Frequency Coupling in L-DOPA-Induced Dyskinesia. *Frontiers in systems neuroscience*. 2016;10:26.
91. Schiffmann SN, Fisone G, Moresco R, Cunha RA, Ferré S. Adenosine A2A receptors and basal ganglia physiology. *Progress in neurobiology*. 2007;83(5):277–292.
92. Buxton D, Bracci E, Overton PG, Gurney K. Striatal neuropeptides enhance selection and rejection of sequential actions. *Frontiers in computational neuroscience*. 2017;11:62.
93. Berke JD. Uncoordinated firing rate changes of striatal fast-spiking interneurons during behavioral task performance. *The Journal of neuroscience : the official journal of the Society for Neuroscience*. 2008;28(40):10075–10080.
94. Kulik JM, Pawlak AP, Kalkat M, Coffey KR, West MO, Mark O, et al. Representation of the body in the lateral striatum of the freely moving rat: Fast Spiking Interneurons respond to stimulation of individual body parts. *Brain Research*. 2018;1657:101–108.
95. Lau T, Gage GJ, Berke JD, Zochowski M. Local dynamics of gap-junction-coupled interneuron networks. *Physical Biology*. 2010;7(1):016015.
96. Mahon S, Vautrelle N, Pezard L, Slaght SJ, Deniau JM, Chouvet G, et al. Distinct patterns of striatal medium spiny neuron activity during the natural sleep-wake cycle. *The Journal of neuroscience : the official journal of the Society for Neuroscience*. 2006;26(48):12587–95. doi:10.1523/JNEUROSCI.3987-06.2006.
97. Taverna S, Ilijic E, Surmeier DJ. Recurrent Collateral Connections of Striatal Medium Spiny Neurons Are Disrupted in Models of Parkinson's Disease. *Journal of Neuroscience*. 2008;28(21):5504–5512.

98. Mainen ZF, Sejnowski TJ. Influence of dendritic structure on firing pattern in model neocortical neurons. *Nature*. 1996;382(6589):363–366.  
doi:10.1038/382363a0.
99. Graveland GA, Williams RS, DiFiglia M. Evidence for degenerative and regenerative changes in neostriatal spiny neurons in Huntington's disease. *Science (New York, NY)*. 1985;227(4688):770–3.
100. Tepper JM, Koós T, Wilson CJ. GABAergic microcircuits in the neostriatum. *Trends in Neurosciences*. 2004;27(11):662–669.
101. Bokil H, Purpura K, Schoffelen JM, Thomson D, Mitra P. Comparing spectra and coherences for groups of unequal size. *Journal of Neuroscience Methods*. 2007;159(2):337–345.
102. Sherfey JS, Soplata AE, Ardid S, Roberts EA, Stanley DA, Pittman-Polletta BR, et al. DynaSim: A MATLAB Toolbox for Neural Modeling and Simulation. *Frontiers in Neuroinformatics*. 2018;12:10. doi:10.3389/fninf.2018.00010.

## Figures and Tables

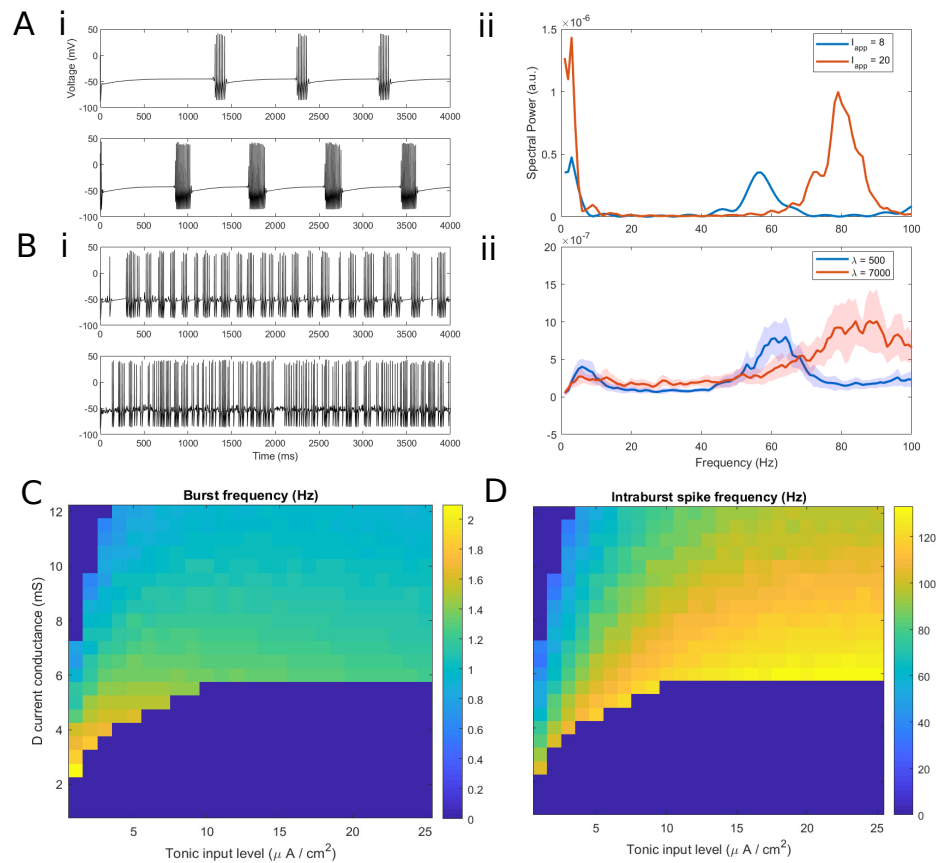
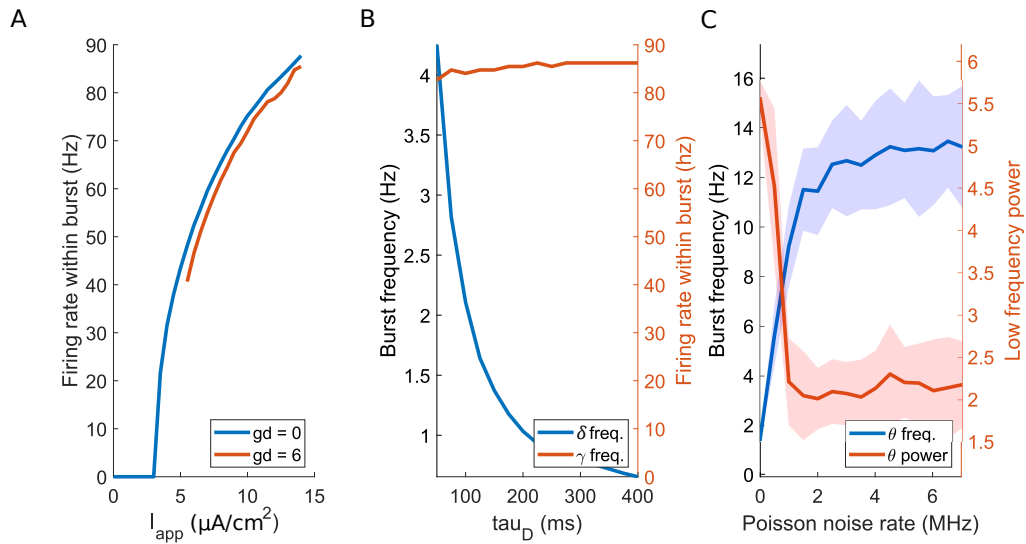
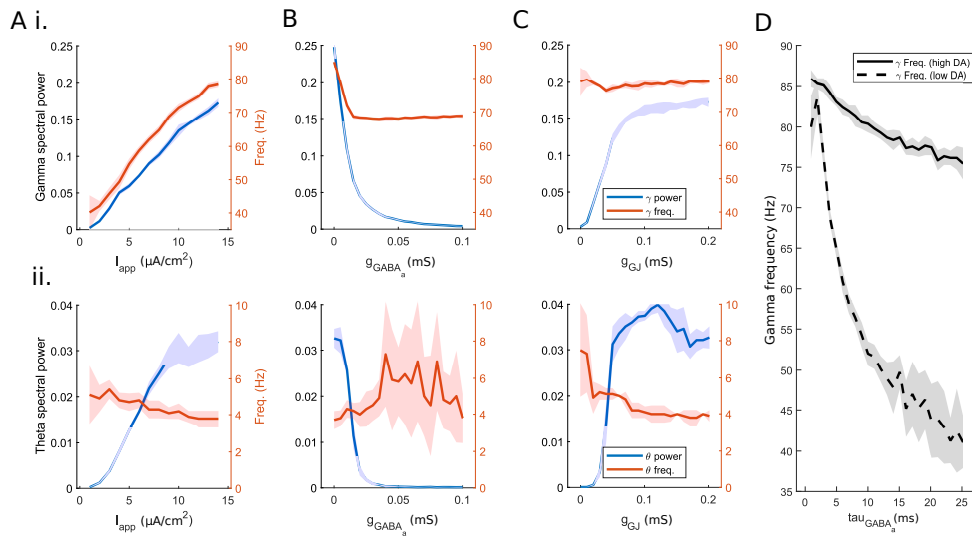


Fig 1. Figure 1



**Fig 2.** Figure 2



**Fig 3.** Figure 3

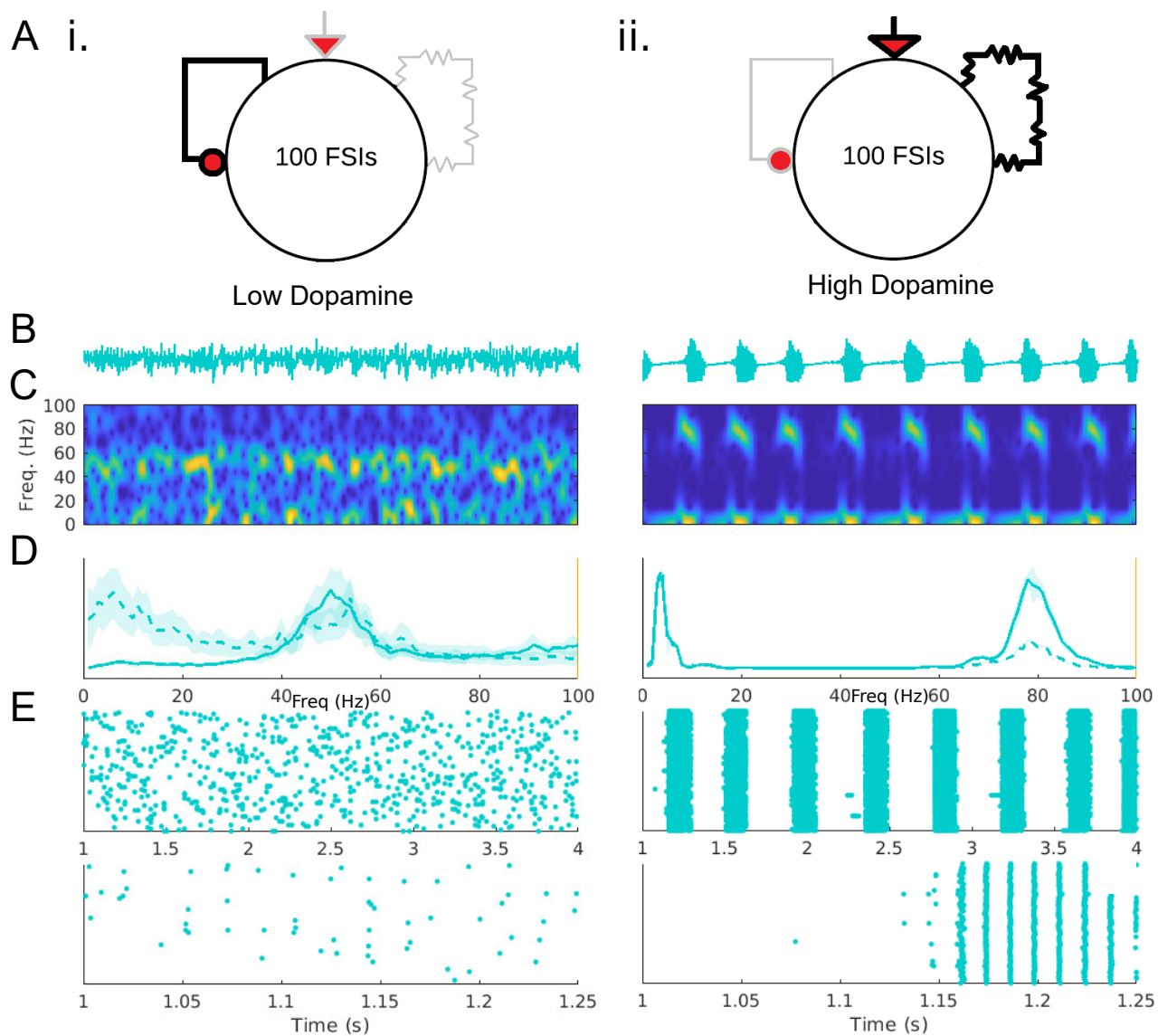


**Fig 4.** Figure 4

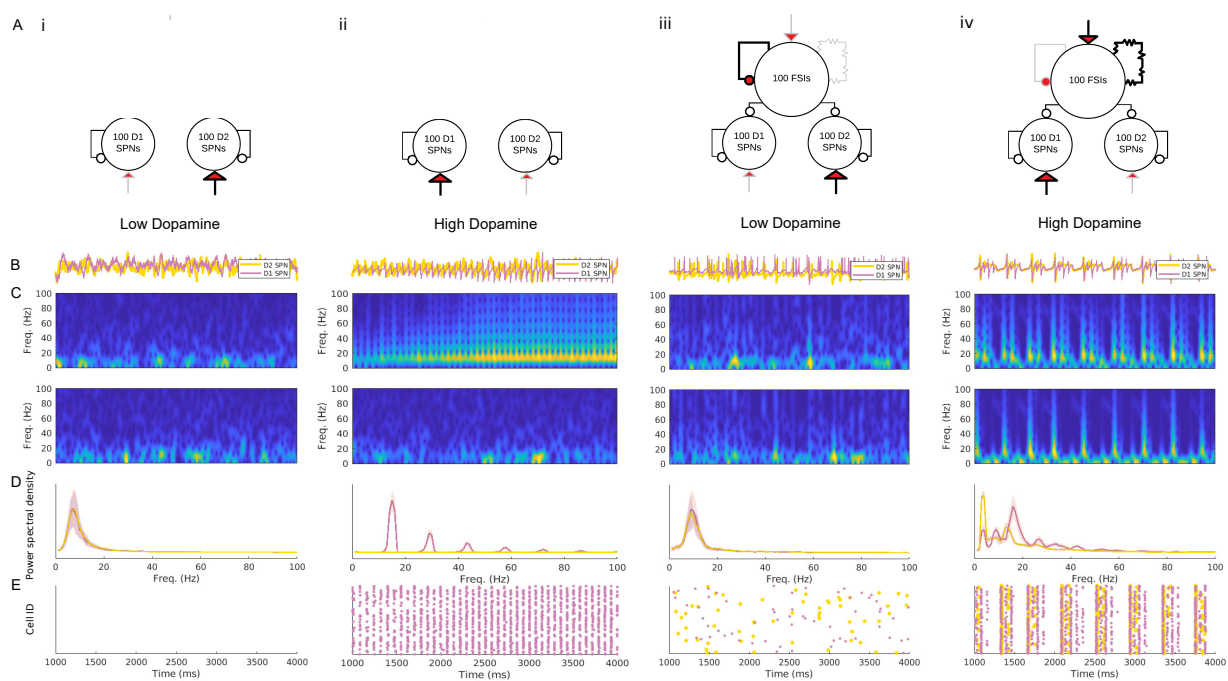
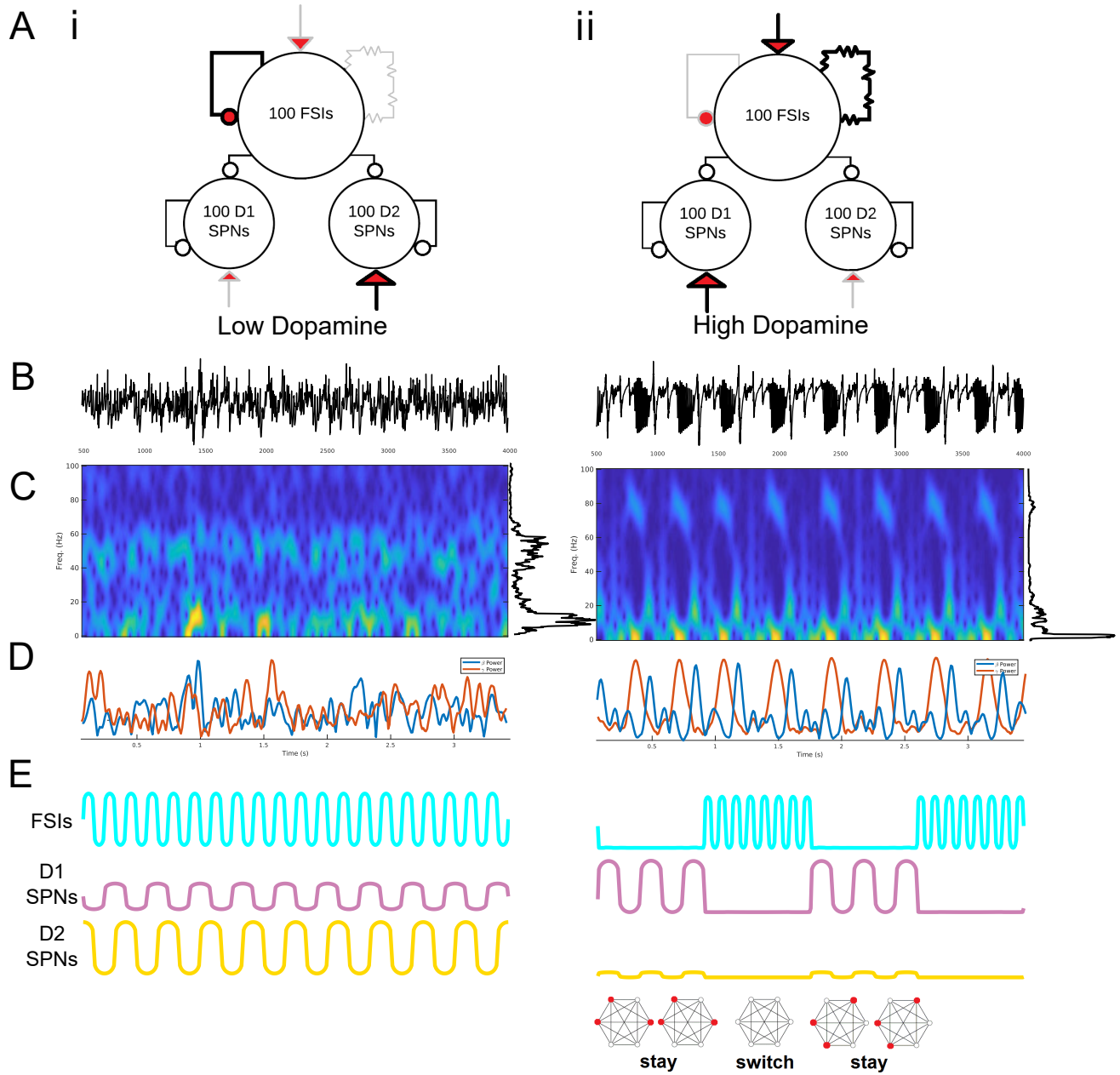


Fig 5. Figure 5





**Fig 6.** Figure 6